

Optimal and Robust Waveform Design for MIMO-OFDM Channel Sensing: A Cramér-Rao Bound Perspective

Xinyang Li^{*†}, Vlad C. Andrei^{*‡}, Ullrich J. Mönich^{*§} and Holger Boche^{*¶}

^{*}Chair of Theoretical Information Technology, Technical University of Munich, Munich, Germany

^{*}BMBF Research Hub 6G-life, [¶]Munich Center for Quantum Science and Technology, [¶]Munich Quantum Valley

Email: [†]xinyang.li@tum.de, [‡]vlad.andrei@tum.de, [§]moenich@tum.de, [¶]boche@tum.de

Abstract—Wireless channel sensing is one of the key enablers for integrated sensing and communication (ISAC) which helps communication networks understand the surrounding environment. In this work, we consider MIMO-OFDM systems and aim to design optimal and robust waveforms for accurate channel parameter estimation given allocated OFDM resources. The Fisher information matrix (FIM) is derived first, and the waveform design problem is formulated by maximizing the log determinant of the FIM. We then consider the uncertainty in the parameters and state the stochastic optimization problem for a robust design. We propose the Riemannian Exact Penalty Method via Smoothing (REPMS) and its stochastic version SREPMS to solve the constrained non-convex problems. In simulations, we show that the REPMS yields comparable results to the semidefinite relaxation (SDR) but with a much shorter running time. Finally, the designed robust waveforms using SREPMS are investigated, and are shown to have a good performance under channel perturbations.

Index Terms—MIMO-OFDM, channel sensing, Cramér-Rao Bound, integrated sensing and communication

I. INTRODUCTION

Since the deployment and evolution of the fifth generation (5G) communications technology, the reliability and connectivity of wireless systems have been improved impressively. Thanks to the large bandwidth at high radio frequencies [1] and the orthogonal frequency-division multiplexing (OFDM) techniques, current networks can provide enormous data rates and serve massive number of users at the same time. Multi-input-multi-output (MIMO) techniques, on the other hand, are used to take advantage of additional spatial degrees of freedom (DoFs) so that the use scenarios are further expanded.

In future communication systems (Beyond 5G (B5G) and 6G) [2], the functionalities of intelligence and perception are expected to be introduced in order to enhance Quality of Service (QoS) and support more advanced and complicated applications such as the Internet of Things (IoT) [3] and unmanned aerial vehicle (UAV) networks [4]. As a key enabler, integrated sensing and communication (ISAC) [5] opens the eyes of future wireless systems, in which the communication

partners can sense the surrounding environment with the aid of received radio signals. Due to the sparse signal propagation paths at short wavelengths, wireless channels carry a large amount of environmental information and are an important feature that can be exploited. Compared to the conventional channel models that assume rich scattering environments, the beam-space channel model [1], [6] leverages the propagation geometric structure and is determined by a set of multipath parameters, i.e., path gain, path delay, Doppler shift, angle of arrival (AoA) and angle of departure (AoD).

Designing appropriate waveforms is an important step in ISAC systems, as it determines the performance limits the systems can achieve. Different design criteria can be chosen [7] to meet different requirements. For example, the authors of [8] aim to design the beamformer by matching the radar beampattern while satisfying the SINR constraints. For parameter estimation, a well-known performance bound is the Cramér-Rao bound (CRB) [9], which states a lower bound on the mean squared estimation error of any unbiased estimator. Waveform design by optimizing CRB is studied in [10]–[12], but they only focus on a subset of multipath parameters and rarely consider the MIMO-OFDM case. In addition, the robustness of the designed waveforms to the changing environment is another important criterion in practice but lacks formulation and analysis in related works. Moreover, the formulated optimization problems of waveform design are generally non-convex. Classical convex relaxation approaches, such as semidefinite relaxation (SDR) [13], suffer from high computational complexity, especially for stochastic optimization. Riemannian manifold methods [8], on the other hand, converge faster than SDR, but require further investigation and appropriate algorithms when additional constraints are present.

In this work, we derive the Fisher information matrix (FIM), the inverse of CRB, of multipath parameters and formulate the optimization problems to design optimal and robust sensing waveforms compatible with current MIMO-OFDM communication systems. We adopt the Riemannian Exact Penalty Method via Smoothing (REPMS) [14] and develop its stochastic version Stochastic Riemannian Exact Penalty Method via Smoothing (SREPMS) to solve the problems. In numerical experiments, the running time of the proposed algorithms and the performance of resulting waveforms are analyzed.

The authors were supported in part by the German Federal Ministry of Education and Research (BMBF) in the programme “Souverän. Digital. Vernetzt.” within the research hub 6G-life under Grant 16KISK002. U. Mönich and H. Boche were supported in part by the BMBF within the project “Post Shannon Communication - NewCom” under Grant 16KIS1003K.

II. SYSTEM MODEL

Considering a MIMO-OFDM communication system comprising a transmitter (Tx) and a receiver (Rx), each of which is equipped with a half wavelength spacing uniform linear array (ULA) with N_T and N_R antenna elements respectively, the frequency representation of the channel matrix [6] consisting of L paths at subcarrier n and OFDM symbol k is

$$\mathbf{H}_{n,k} = \sum_{l=1}^L b_l \omega_{n,k,l} \mathbf{a}_R(\phi_l) \mathbf{a}_T(\theta_l)^\top, \quad (1)$$

with $\omega_{n,k,l} = e^{-j2\pi n f_0 \tau_l} e^{j2\pi f_{D,l} k T_s}$, where

- f_0 is the OFDM subcarrier spacing,
- T_s is the OFDM symbol duration,
- $b_l \in \mathbb{C}$ is the channel gain of the l -th path,
- τ_l is the l -th path delay,
- $f_{D,l}$ is the Doppler shift of the l -th path,
- $\mathbf{a}_T(\theta_l) \in \mathbb{C}^{N_T}$ is the ULA response vector at AoD θ_l ,
- $\mathbf{a}_R(\phi_l) \in \mathbb{C}^{N_R}$ is the ULA response vector at AoA ϕ_l .

Suppose the Tx transmits signal $\mathbf{x}_{n,k}$ at the (n, k) -th OFDM resource element (RE), then the received signal is

$$\mathbf{y}_{n,k} = \mathbf{H}_{n,k} \mathbf{x}_{n,k} + \mathbf{z}_{n,k}, \quad (2)$$

with $\mathbf{z}_{n,k}$ being the additive Gaussian noise of zero mean and covariance matrix $\mathbf{C}_{\mathbf{z}_{n,k}} = \sigma_{n,k}^2 \mathbf{I}$. The noise vectors on different REs are assumed to be independent.

Compared to the classical channel estimation, where only the channel matrices $\mathbf{H}_{n,k}$ are of interest, in future networks it will be vital to additionally extract their multipath information [5], i.e., $\{b_l, \tau_l, f_{D,l}, \phi_l, \theta_l\}$ for all l . To this end, the waveforms $\mathbf{x}_{n,k}$ should be designed carefully for accurate parameter estimation. In OFDM, the sensing waveforms can either be designed jointly with the communication symbols, or allocated to the dedicated REs and designed independently of the communication symbols. In this work, we focus on the latter case, as its implementation is compatible with current standards such as 5G NR [12], where the REs are not always fully occupied.

A. Cramér-Rao Bound (CRB)

Given the observation \mathbf{y} that depends on the parameter $\boldsymbol{\xi}$ to be estimated and the conditioned distribution $p(\mathbf{y}|\boldsymbol{\xi})$, the mean squared error (MSE) of any unbiased estimator $\hat{\boldsymbol{\xi}}(\mathbf{y})$ is bounded by the inverse of the FIM \mathcal{I} , i.e., $\mathbb{E}[(\hat{\boldsymbol{\xi}}(\mathbf{y}) - \boldsymbol{\xi})(\hat{\boldsymbol{\xi}}(\mathbf{y}) - \boldsymbol{\xi})^\text{H}] \succeq \mathcal{I}^{-1}$ and $\mathbf{P} \succeq \mathbf{Q}$ indicates that $\mathbf{P} - \mathbf{Q}$ is a positive semidefinite (PSD) matrix [9], [15] for two PSD matrices \mathbf{P} and \mathbf{Q} . When $p(\mathbf{y}|\boldsymbol{\xi})$ is a complex Gaussian distribution [9], the value at the i -th row and j -th column of FIM is

$$\begin{aligned} [\mathcal{I}]_{i,j} = & \text{Tr} \left[\mathbf{C}_y^{-1}(\boldsymbol{\xi}) \frac{\partial \mathbf{C}_y(\boldsymbol{\xi})}{\partial \xi_i} \mathbf{C}_y^{-1}(\boldsymbol{\xi}) \frac{\partial \mathbf{C}_y(\boldsymbol{\xi})}{\partial \xi_j} \right] \\ & + 2\text{Re} \left[\frac{\partial \boldsymbol{\mu}^\text{H}(\boldsymbol{\xi})}{\partial \xi_i} \mathbf{C}_y^{-1}(\boldsymbol{\xi}) \frac{\partial \boldsymbol{\mu}(\boldsymbol{\xi})}{\partial \xi_j} \right], \end{aligned} \quad (3)$$

where ξ_i denotes the i -th component of $\boldsymbol{\xi}$, and $\boldsymbol{\mu}(\boldsymbol{\xi})$, $\mathbf{C}_y(\boldsymbol{\xi})$ are the corresponding mean and covariance matrix of \mathbf{y}

dependent on $\boldsymbol{\xi}$. $\text{Tr}[\cdot]$ and $\text{Re}[\cdot]$ indicate the trace and real part of a complex matrix respectively. Rewriting (2) using the vectorization formula $\text{vec}(\mathbf{ABC}) = (\mathbf{C}^\top \otimes \mathbf{A})\text{vec}(\mathbf{B})$ with the Kronecker product \otimes results in

$$\mathbf{y}_{n,k} = (\mathbf{x}_{n,k}^\top \otimes \mathbf{I}) \mathbf{h}_{n,k} + \mathbf{z}_{n,k}, \quad (4)$$

in which \mathbf{I} is the identity matrix and

$$\mathbf{h}_{n,k} = \text{vec}(\mathbf{H}_{n,k}) = \sum_{l=1}^L b_l \omega_{n,k,l} \mathbf{a}_T(\theta_l) \otimes \mathbf{a}_R(\phi_l). \quad (5)$$

We assume that the multipath parameters are independent on (n, k) . Without loss of generality, we allocate sensing symbols on M OFDM REs, say, $\{(n_m, k_m)\}_{m=1}^M$. In the following, we use subscript m to indicate (n_m, k_m) for convenience. To express the dependence of the channel on the parameters explicitly, we write \mathbf{h}_m as $\mathbf{h}_m(\boldsymbol{\xi})$, with $\boldsymbol{\xi} = \text{vec}([\xi_1, \xi_2, \dots, \xi_L]^\top)$ collecting all multipath parameters,

$$\boldsymbol{\xi}_l = [b_{l,R} \quad b_{l,I} \quad \tau_l \quad f_{D,l} \quad \phi_l \quad \theta_l]^\top, \quad (6)$$

and $b_{l,R}$ and $b_{l,I}$ denote the real and imaginary part b_l , respectively. Therefore, (3) can be rewritten as

$$[\mathcal{I}]_{i,j} = \sum_{m=1}^M \frac{2}{\sigma_m^2} \text{Re} \left[\left(\frac{\partial \mathbf{h}_m(\boldsymbol{\xi})}{\partial \xi_i} \right)^\text{H} (\mathbf{x}_m^* \mathbf{x}_m^\top \otimes \mathbf{I}) \frac{\partial \mathbf{h}_m(\boldsymbol{\xi})}{\partial \xi_j} \right], \quad (7)$$

where we use the mixed-product property of Kronecker product. The resulting FIM is derived in Appendix A as

$$\mathcal{I} = \text{Re} \left[\left(\sum_{m=1}^M \frac{2}{\sigma_m^2} \boldsymbol{\Lambda}_m^\text{H} \mathbf{T}^\text{H} \mathbf{x}_m^* \mathbf{x}_m^\top \mathbf{T} \boldsymbol{\Lambda}_m \right) \circ (\mathbf{R}^\text{H} \mathbf{R}) \right], \quad (8)$$

where \circ indicates the Hadamard product, and $\boldsymbol{\Lambda}_m$, \mathbf{T} , \mathbf{R} depend on the parameters and are given in (15).

B. Optimal Design

There are several ways to construct objective functions on \mathcal{I} to be optimized so that the CRB is correspondingly minimized [10]. We choose to maximize the determinant of FIM since it controls the element scaling while calculating the matrix inverse. In addition, depending on different use cases, we need to place more importance on certain parameters, e.g., delays and AoAs are much more relevant for indoor localization [16]. To this end, we can multiply \mathcal{I} with a weighting matrix \mathbf{J} from the right and its conjugate transpose \mathbf{J}^H from the left to scale the associated parts. By imposing the power constraints and defining $\mathbf{X} = [\mathbf{x}_1, \mathbf{x}_2, \dots, \mathbf{x}_M]$, the overall optimization problem can be expressed as

$$\begin{aligned} & \max_{\mathbf{X}} \log \det (\mathbf{J}^\text{H} \mathcal{I} \mathbf{J}) \\ \text{s.t.} \quad & \frac{1}{M} \text{Tr}[\mathbf{X} \mathbf{X}^\text{H}] \leq P \\ & \|\mathbf{x}_m\|_2^2 \leq P_m, \quad \forall m = 1 \dots M. \end{aligned} \quad (\text{P1})$$

(P1) is a nonconvex problem and can be solved using the SDR technique, but the number of variables in the relaxed problem increases quadratically with the number of transmit antennas

N_T , resulting in a high computational load. To alleviate this problem, we observe that the total power is always exhausted to reach a higher objective value. Hence, the total power inequality constraint in (P1) can then be replaced by equality, which leads to the hypersphere manifold

$$\mathcal{S} = \left\{ \mathbf{X} \in \mathbb{C}^{N_T \times M} \mid \text{Tr}[\mathbf{X}\mathbf{X}^H] = \|\mathbf{X}\|_F^2 = MP \right\}, \quad (9)$$

and the resulting problem is reformulated as a constrained manifold optimization problem in the following:

$$\begin{aligned} & \max_{\mathbf{X} \in \mathcal{S}} \log \det(\mathbf{J}^H \mathcal{I} \mathbf{J}) \\ \text{s.t.} \quad & \|\mathbf{x}_m\|^2 \leq P_m, \quad \forall m = 1 \dots M. \end{aligned} \quad (\text{P1M})$$

C. Robust Design

It should be mentioned that the objective function in the optimal design problem depends on ξ through \mathcal{I} . A full and precise knowledge of the parameters can result in optimal waveforms. However, in practice, such assumption is unrealistic, due to, for instance, the changing of environment, parameter estimation error and feedback delay. To this end, we assume that the Tx only knows the perturbed parameters $\hat{\xi}$, while the true value $\xi = \hat{\xi} + \Delta\xi$ is unavailable. The error $\Delta\xi$ follows the Gaussian distribution $\mathcal{N}(\mathbf{0}, \mathbf{C}_e)$, with a diagonal covariance matrix \mathbf{C}_e comprising diagonal elements $\sigma_{b_{i,R}}^2, \sigma_{b_{i,I}}^2, \sigma_{\tau_i}^2, \sigma_{f_{D,i}}^2, \sigma_{\phi_i}^2, \sigma_{\theta_i}^2$ for all l corresponding to the error variances of respective parameters. The unknown true parameter ξ thus follows $\mathcal{N}(\hat{\xi}, \mathbf{C}_e)$. In the following, we also take into account the uncertainty in the error variances and assume they are randomly distributed.

From the perspective of robust optimization [17], one option is to optimize over the expectation of the objective function. Thus, the robust design problem can be formulated as

$$\begin{aligned} & \max_{\mathbf{X} \in \mathcal{S}} \mathbb{E}[\log \det(\mathbf{J}^H \mathcal{I} \mathbf{J})] \\ \text{s.t.} \quad & \|\mathbf{x}_m\|^2 \leq P_m, \quad \forall m = 1 \dots M, \end{aligned} \quad (\text{P1E})$$

with \mathbb{E} taken over \mathbf{C}_e and ξ . One issue to solve (P1E) is that it's intractable to derive the closed form of the objective function. A common approach is to apply the stochastic method by sampling points randomly and calculating the empirical mean value as an approximation, which will be discussed in III-C.

III. OPTIMIZATION

A. Semidefinite Relaxation

We introduce the new variables $\mathbf{R}_m = \mathbf{x}_m^* \mathbf{x}_m^\top$ for all m , relax its rank 1 constraint and the optimization problem (P1) becomes

$$\begin{aligned} & \max_{\mathbf{R}_1, \mathbf{R}_2, \dots, \mathbf{R}_M} \log \det(\mathbf{J}^H \mathcal{I} \mathbf{J}) \\ \text{s.t.} \quad & \frac{1}{M} \text{Tr} \left[\sum_{m=1}^M \mathbf{R}_m \right] \leq P \\ & \mathbf{R}_m \succeq \mathbf{0}, \quad \text{Tr}[\mathbf{R}_m] \leq P_m, \quad \forall m = 1, \dots, M, \end{aligned} \quad (\text{P1R})$$

which is shown as semidefinite programming (SDP). After solving (P1R), one can approximate the rank 1 results by singular value decomposition (SVD) or randomization [13].

B. Manifold Optimization

Due to the additional constraints on the symbol norm, the traditional unconstrained methods like Riemannian conjugate gradient (RCG) [8] cannot be directly applied. We therefore modify the problem by adding the constraint as a penalty term to the objective function. Specifically, we employ the REPMS [14], in which the problem (P1M) can be reformulated as

$$\begin{aligned} & \min_{\mathbf{X} \in \mathcal{S}} \mathcal{L}(\mathbf{X}, \rho, u) = \\ & - \log \det(\mathbf{J}^H \mathcal{I} \mathbf{J}) + \rho \sum_{m=1}^M p_u(\|\mathbf{x}_m\|_2^2 - P_m), \end{aligned} \quad (10)$$

with ρ, u being the penalty weight, smoothing factor respectively, and the linear-quadratic loss is given by

$$p_u(x) = \begin{cases} 0 & x \leq 0 \\ \frac{x^2}{2u} & 0 \leq x \leq u \\ x - \frac{u}{2} & x \geq u \end{cases} \quad (11)$$

Choosing RCG as the base solver, we end up with the REPMS [14] in Algorithm 1 for optimal waveform design. At the k -th step, the update direction \mathbf{p}_k is computed based on the previous direction and the current Riemannian gradient $\text{grad}\mathcal{L}$ through the function τ , which can be chosen according to different rules [18]. The retraction γ associated to the hypersphere manifold [8] is used as the update function that moves the point \mathbf{X}_k along \mathbf{p}_k and keeps it on \mathcal{S} .

Algorithm 1 Optimal waveform design using REPMS

Input: Function \mathcal{L} , initial point $\mathbf{X}_0 \in \mathcal{S}$, initial penalty weight $\rho_0, \theta_\rho > 1, \rho_{\max}$, initial smoothing factor $u_0, 0 < \theta_u < 1, u_{\min}$

Output: Optimal \mathbf{X}

$k \leftarrow 0$

$\mathbf{p}_0 \leftarrow -\text{grad}\mathcal{L}(\mathbf{X}_0, \rho_0, u_0)$

while Stopping criterion not met **do**

 Compute update step size t_k by certain rules

$\mathbf{X}_{k+1} \leftarrow \gamma(\mathbf{X}_k, \mathbf{p}_k, t_k)$

$\rho_{k+1} \leftarrow \min\{\theta_\rho \rho, \rho_{\max}\}$

$u_{k+1} \leftarrow \max\{\theta_u u, u_{\min}\}$

$\mathbf{p}_{k+1} \leftarrow \tau(\mathbf{p}_k, \text{grad}\mathcal{L}(\mathbf{X}_{k+1}, \rho_{k+1}, u_{k+1}))$

end while

return \mathbf{X}_k

C. Stochastic Optimization

To solve (P1E), we apply the idea of stochastic optimization, in which the expectation is approximated by the sample means using a Monte Carlo approach, namely

$$\frac{1}{N} \sum_{n=1}^N \log \det(\mathbf{J}^H \mathcal{I}_n \mathbf{J}) \approx \mathbb{E}[\log \det(\mathbf{J}^H \mathcal{I} \mathbf{J})], \quad (12)$$

where \mathcal{I}_n is computed on ξ_n with $\xi_n \sim \mathcal{N}(\hat{\xi}, \mathbf{C}_{e,n})$ and the diagonal elements of $\mathbf{C}_{e,n}$ are sampled randomly from the predefined distributions. It should be mentioned that evaluating

the sample mean brings additional computational complexity and SDR might become infeasible in practice for large sample size N thus will not be used to solve the robust design problem in our work.

Similar to Algorithm 1, we reformulate (PIE) to an unconstrained case as

$$\begin{aligned} \min_{\mathbf{X} \in \mathcal{S}} \mathcal{S}\mathcal{L}(\mathbf{X}, \{\xi_n\}_{n=1}^N, \rho, u) = \\ -\frac{1}{N} \sum_{n=1}^N \log \det(\mathbf{J}^H \mathcal{I}_n \mathbf{J}) + \rho \sum_{m=1}^M p_u (\|\mathbf{x}_m\|_2^2 - P_m). \end{aligned} \quad (13)$$

While optimizing, at each new iteration we sample a new set of N parameter vectors to compute the sample mean and apply one step REPMS. Finally, we summarize the SREPMS for robust waveform design in Algorithm 2.

Algorithm 2 Robust waveform design using SREPMS

Input: Function $\mathcal{S}\mathcal{L}$, N , $\hat{\xi}$, distributions of error variances, \mathbf{J} , $\mathbf{X}_0 \in \mathcal{S}$, ρ_0 , $\theta_\rho > 1$, ρ_{\max} , u_0 , $0 < \theta_u < 1$, u_{\min}

Output: Robust \mathbf{X}

Sample $\{\mathbf{C}_{e,n}\}_{n=1}^N$ from the given distributions

Sample ξ_n from $\mathcal{N}(\hat{\xi}, \mathbf{C}_{e,n})$ for $n = 1 \dots N$

$\mathbf{p}_0 \leftarrow -\text{grad}\mathcal{S}\mathcal{L}(\mathbf{X}_0, \{\xi_n\}_{n=1}^N, \rho_0, u_0)$

$k \leftarrow 0$

while Stopping criterion not met **do**

 Compute update step size t_k

$\mathbf{X}_{k+1} \leftarrow \gamma(\mathbf{X}_k, \mathbf{p}_k, t_k)$

 Sample $\{\mathbf{C}_{e,n}\}_{n=1}^N$ from the given distributions

 Sample ξ_n from $\mathcal{N}(\hat{\xi}, \mathbf{C}_{e,n})$ for $n = 1 \dots N$

$\rho_{k+1} \leftarrow \min\{\theta_\rho \rho, \rho_{\max}\}$

$u_{k+1} \leftarrow \max\{\theta_u u, u_{\min}\}$

$\mathbf{p}_{k+1} \leftarrow \tau(\mathbf{p}_k, \text{grad}\mathcal{S}\mathcal{L}(\mathbf{X}_{k+1}, \rho_{k+1}, u_{k+1}))$

$k \leftarrow k + 1$

end while

return \mathbf{X}_k

IV. NUMERICAL RESULTS

In the simulations, we consider an 8×8 MIMO system and set the carrier frequency f_c to 3 GHz and the subcarrier spacing f_0 to 15 kHz. We allocate the sensing waveforms in a rectangular OFDM region, occupying 128 subcarriers and 14 OFDM symbols (one slot in 5G). The average transmit power P and SNR are fixed to 10 and -10 dB, respectively. The symbol-wise power constraint P_m is set to αP , where $\alpha > 1$ for all m . The scaling matrix \mathbf{J} is a diagonal matrix with the diagonal elements $T_s = \frac{1}{f_0}$ and f_0 for the path delay and Doppler shift parts, respectively, and 1 otherwise, to avoid the numerical instability caused by the large difference in the orders of the values in \mathcal{I} . The number of channel paths is set to 3, and we generate 100 realizations of multipath parameters randomly according to the following settings:

- The real and imaginary parts of path gains are from zero mean unit variance normal distribution,

- By sampling the path lengths from a uniform distribution between 10 and 800 meters, the path delays are computed,
- By sampling the relative velocities of different paths from a uniform distribution between 0 and 80 m/s, the Doppler shifts are computed,
- AoAs and AoDs are sampled uniformly between -90° and 90° .

In the following, the optimization tool MOSEK [19] is used for SDR while REPMS and SREPMS are implemented with Pymanopt [20].

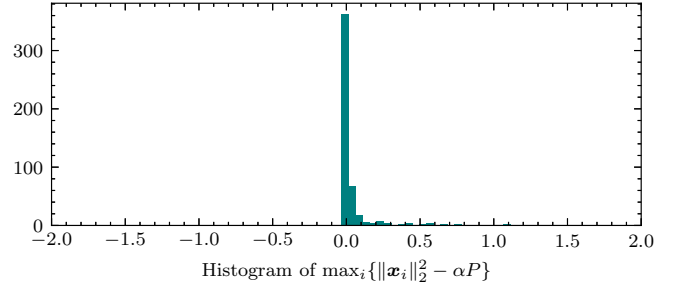


Fig. 1: Histogram of the maximum symbol norm resulting from REPMS subtracted by the threshold.

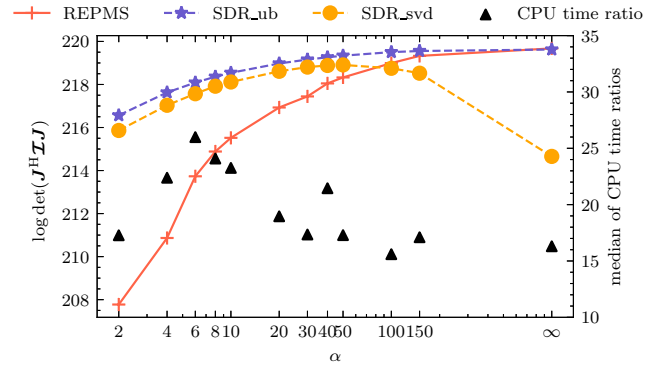


Fig. 2: Comparison of optimization results and the CPU time ratios (SDR to REPMS). **ub** (upper bound) and **svd** indicate the SDR solutions without and with SVD rank 1 recovery.

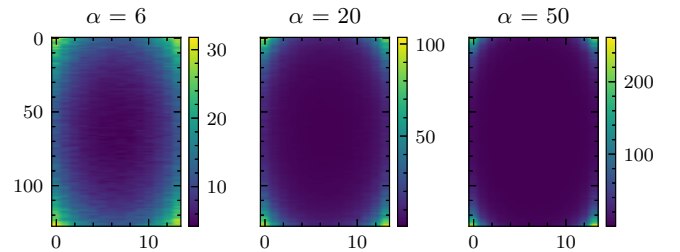


Fig. 3: Resulting average power allocation of REPMS.

We first investigate the feasibility of the REPMS results. The associated parameters are $\rho_0 = 1$, $u_0 = 1$, $u_{\min} = 10^{-6}$ and $\theta_u = (u_{\min}/u_0)^{\frac{1}{50}}$ by following the experiment settings in

[14]. ρ_{\max} should be as large as possible but the numerical overflow need to be avoided thus is set to 2^{20} . We also choose $\theta_\rho = 2$ as it yields a faster convergence in simulations. We apply Algorithm 1 to the generated channel realizations and plot the histogram of the differences between the resulting maximum symbol power with the threshold αP , i.e., $\max_i \{\|\mathbf{x}_i\|_2^2 - \alpha P\}$, for $\alpha = 2, 4, 6, 8, 10$ in Fig. 1. It turns out that REPMS can lead to feasible solutions when a small tolerance allowed.

To compare the performance between SDR and REPMS, the averaged optimized objective values and the medians of consumed central processing unit (CPU) time ratios (SDR to REPMS) are plotted in Fig. 2 for varying α (∞ means no symbol-wise constraint). It's obvious that the SDR method produces larger objective values for low values of α . After a certain threshold, the REPMS outperforms the SDR with SVD recovery and even reaches the SDR upper bound despite the fact that the REPMS algorithm can achieve more than 15 times speedup than SDR in terms of CPU time on the same hardware platform, which makes the manifold optimization more attractive in our works. We also demonstrate the average power allocation on the given OFDM resources in Fig. 3, and notice that most power is concentrated on few REs at the grid corners, so the designed sensing waveforms are expected to have little impact on the communication resources.

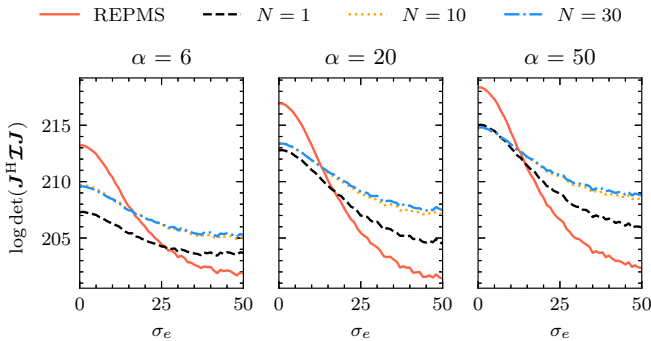


Fig. 4: Performance of designed robust waveforms using SREPMS.

To test the performance of the designed robust waveforms, we use a single parameter σ_e to adjust the variances of all multipath parameters. In particular, we set the parameter perturbation variances as $\sigma_{b_{l,R}} = \sigma_{b_{l,I}} = 10^{-2}\sigma_e$, $\sigma_{\tau_l} = 10^{-8}\sigma_e$, $\sigma_{f_{D,l}} = 5\sigma_e$, $\sigma_{\phi_l} = \sigma_{\theta_l} = 10^{-2}\sigma_e$ for all l and σ_e is uniformly distributed from 0 to 50 ($\sigma_e = 0$ means no perturbation). We apply Algorithm 2 by treating the previously generated 100 parameters as $\hat{\xi}$ and set N to 1, 10 and 30. To test the performance of different waveforms, for each fixed $\hat{\xi}$ and σ_e , we generate another 100 random parameters as the true ξ from $\mathcal{N}(\hat{\xi}, C_e)$. The resulting average objective values against σ_e are plotted in Fig. 4. It shows that as N increases, the designed waveforms yield better performance, but at the cost of efficiency, as expected. We also observe a trade-off between the designed optimal and robust waveforms

for different levels of uncertainty. Furthermore, the feasibility and power allocation of the SREPMS results are similar to REPMS. Due to the page limitation, we don't demonstrate them here.

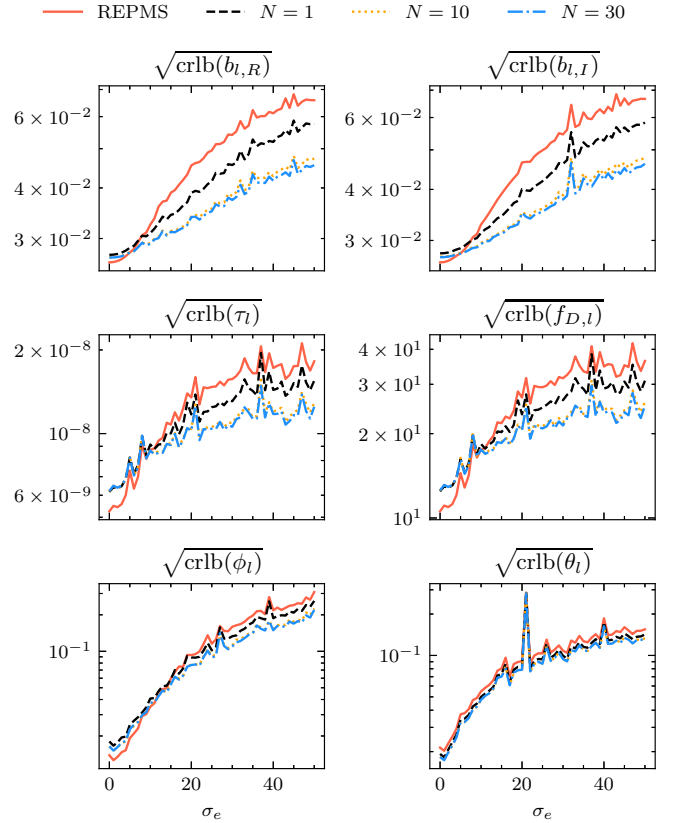


Fig. 5: CRB of multipath parameters resulting from previously designed waveforms at different perturbation levels.

Finally, we plot the resulting square root of the CRB for each parameter against varying channel perturbation levels σ_e in Fig. 5 for $\alpha = 50$. For the same type of parameter, we take their average over all paths. The nonsmooth curves reflect that a larger log det of FIM can't always guarantee a lower CRB on every parameter, but the overall results are shown to be consistent with the previous observations.

V. CONCLUSION

In this paper, we derive the CRB for the multipath parameter estimation in MIMO-OFDM channel sensing. We formulate the waveform design problems to maximize the log det of FIM under total and symbol-wise power constraints and introduce REPMS to design optimal waveforms. By considering the uncertainty of parameters, the stochastic method SREPMS for robust waveform design is then proposed. In numerical simulations, it shows that the manifold techniques can speed up the solving process over 15 times in terms of CPU time and can still provide comparable results to SDR. Finally, the performance trade-off of robust waveforms is demonstrated and the resulting CRB for each parameter is presented.

$$\begin{aligned}
\Lambda_m &= \text{diag}\{\dots \omega_{m,l} \dots j\omega_{m,l} \dots b_l g_{m,l} \dots b_l f_{m,l} \dots b_l \omega_{m,l} \dots b_l \omega_{m,l} \dots\}, \quad l = 1 \dots L, \\
\mathbf{T} &= [\mathbf{A}_T(\boldsymbol{\theta}) \quad \mathbf{A}_T(\boldsymbol{\theta}) \quad \mathbf{A}_T(\boldsymbol{\theta}) \quad \mathbf{A}_T(\boldsymbol{\theta}) \quad \mathbf{A}_T(\boldsymbol{\theta}) \quad \mathbf{D}_T(\boldsymbol{\theta})], \\
\mathbf{R} &= [\mathbf{A}_R(\boldsymbol{\phi}) \quad \mathbf{A}_R(\boldsymbol{\phi}) \quad \mathbf{A}_R(\boldsymbol{\phi}) \quad \mathbf{A}_R(\boldsymbol{\phi}) \quad \mathbf{D}_R(\boldsymbol{\phi}) \quad \mathbf{A}_R(\boldsymbol{\phi})], \\
\mathbf{A}_T(\boldsymbol{\theta}) &= [\mathbf{a}_T(\theta_1) \quad \mathbf{a}_T(\theta_2) \quad \dots \quad \mathbf{a}_T(\theta_L)], \quad \mathbf{D}_T(\boldsymbol{\theta}) = [\mathbf{d}_T(\theta_1) \quad \mathbf{d}_T(\theta_2) \quad \dots \quad \mathbf{d}_T(\theta_L)], \\
\mathbf{A}_R(\boldsymbol{\phi}) &= [\mathbf{a}_R(\phi_1) \quad \mathbf{a}_R(\phi_2) \quad \dots \quad \mathbf{a}_R(\phi_L)], \quad \mathbf{D}_R(\boldsymbol{\phi}) = [\mathbf{d}_R(\phi_1) \quad \mathbf{d}_R(\phi_2) \quad \dots \quad \mathbf{d}_R(\phi_L)].
\end{aligned} \tag{15}$$

APPENDIX A

The derivative of $\mathbf{h}_m(\boldsymbol{\xi})$ to each parameter are given as

$$\begin{aligned}
\frac{\partial \mathbf{h}_m(\boldsymbol{\xi})}{\partial b_{l,R}} &= \omega_{m,l} \mathbf{a}_T(\theta_l) \otimes \mathbf{a}_R(\phi_l) \\
\frac{\partial \mathbf{h}_m(\boldsymbol{\xi})}{\partial b_{l,I}} &= j\omega_{m,l} \mathbf{a}_T(\theta_l) \otimes \mathbf{a}_R(\phi_l) \\
\frac{\partial \mathbf{h}_m(\boldsymbol{\xi})}{\partial \tau_l} &= b_l g_{m,l} \mathbf{a}_T(\theta_l) \otimes \mathbf{a}_R(\phi_l) \\
\frac{\partial \mathbf{h}_m(\boldsymbol{\xi})}{\partial f_{D,l}} &= b_l f_{m,l} \mathbf{a}_T(\theta_l) \otimes \mathbf{a}_R(\phi_l) \\
\frac{\partial \mathbf{h}_m(\boldsymbol{\xi})}{\partial \phi_l} &= b_l \omega_{m,l} \mathbf{a}_T(\theta_l) \otimes \mathbf{d}_R(\phi_l) \\
\frac{\partial \mathbf{h}_m(\boldsymbol{\xi})}{\partial \theta_l} &= b_l \omega_{m,l} \mathbf{d}_T(\theta_l) \otimes \mathbf{a}_R(\phi_l)
\end{aligned}$$

with $g_{m,l} = -j2\pi n_m f_0 \omega_{m,l}$, $f_{m,l} = j2\pi k_m T_s \omega_{m,l}$, $\mathbf{d}_R(\phi_l) = \frac{\partial \mathbf{a}_R(\phi_l)}{\partial \phi_l}$ and $\mathbf{d}_T(\theta_l) = \frac{\partial \mathbf{a}_T(\theta_l)}{\partial \theta_l}$. It's then straightforward to show that $\frac{\partial \mathbf{h}_m(\boldsymbol{\xi})}{\partial \boldsymbol{\xi}} = \mathbf{T} * \mathbf{R} \Lambda_m$ where $*$ is the Kahtri-Rao product (column-wise Kronecker product), and the respective matrices are given in (15). We define \bullet as the face-splitting product (row-wise Kronecker product). Given matrices $\mathbf{A}, \mathbf{B}, \mathbf{C}, \mathbf{D}, \mathbf{E}, \mathbf{F}$ we have the following properties:

- $(\mathbf{A} * \mathbf{B})^H = \mathbf{A}^H \bullet \mathbf{B}^H$,
- $(\mathbf{A} \bullet \mathbf{B})(\mathbf{C} \bullet \mathbf{D})(\mathbf{E} * \mathbf{F}) = (\mathbf{ACE}) \circ (\mathbf{BDF})$,
- $\mathbf{A} \circ (\mathbf{BDF}) = (\mathbf{BAF}) \circ \mathbf{D}$ if \mathbf{B} and \mathbf{F} are diagonal matrices,
- $\mathbf{A} \circ \mathbf{B} + \mathbf{C} \circ \mathbf{B} = (\mathbf{A} + \mathbf{C}) \circ \mathbf{B}$.

With these properties the FIM can be derived as

$$\begin{aligned}
\mathcal{I} &= \sum_{m=1}^M \frac{2}{\sigma_m^2} \text{Re} \left[(\mathbf{T} * \mathbf{R} \Lambda_m)^H (\mathbf{x}_m^* \mathbf{x}_m^T \otimes \mathbf{I}) (\mathbf{T} * \mathbf{R} \Lambda_m) \right] \\
&= \sum_{m=1}^M \frac{2}{\sigma_m^2} \text{Re} \left[(\mathbf{T}^H \mathbf{x}_m^* \mathbf{x}_m^T \mathbf{T}) \circ (\Lambda_m^H \mathbf{R}^H \mathbf{R} \Lambda_m) \right] \\
&= \text{Re} \left[\sum_{m=1}^M \left(\frac{2}{\sigma_m^2} \Lambda_m^H \mathbf{T}^H \mathbf{x}_m^* \mathbf{x}_m^T \mathbf{T} \Lambda_m \right) \circ (\mathbf{R}^H \mathbf{R}) \right].
\end{aligned} \tag{14}$$

REFERENCES

- [1] R. W. Heath, N. González-Prelcic, S. Rangan, W. Roh, and A. M. Sayeed, "An overview of signal processing techniques for millimeter wave mimo systems," *IEEE Journal of Selected Topics in Signal Processing*, vol. 10, no. 3, pp. 436–453, 2016.
- [2] W. Saad, M. Bennis, and M. Chen, "A vision of 6G wireless systems: Applications, trends, technologies, and open research problems," *IEEE Network*, vol. 34, no. 3, pp. 134–142, 2020.
- [3] S. He, K. Shi, C. Liu, B. Guo, J. Chen, and Z. Shi, "Collaborative sensing in internet of things: A comprehensive survey," *IEEE Communications Surveys & Tutorials*, 2022.
- [4] Y. Zeng, Q. Wu, and R. Zhang, "Accessing from the sky: A tutorial on UAV communications for 5G and beyond," *Proceedings of the IEEE*, vol. 107, no. 12, pp. 2327–2375, 2019.
- [5] F. Liu, Y. Cui, C. Masouros, J. Xu, T. X. Han, Y. C. Eldar, and S. Buzzi, "Integrated sensing and communications: Toward dual-functional wireless networks for 6G and beyond," *IEEE Journal on Selected Areas in Communications*, vol. 40, no. 6, pp. 1728–1767, 2022.
- [6] J. A. Zhang, F. Liu, C. Masouros, R. W. Heath, Z. Feng, L. Zheng, and A. Petropulu, "An overview of signal processing techniques for joint communication and radar sensing," *IEEE Journal of Selected Topics in Signal Processing*, vol. 15, no. 6, pp. 1295–1315, 2021.
- [7] A. Liu, Z. Huang, M. Li, Y. Wan, W. Li, T. X. Han, C. Liu, R. Du, D. K. P. Tan, J. Lu *et al.*, "A survey on fundamental limits of integrated sensing and communication," *IEEE Communications Surveys & Tutorials*, vol. 24, no. 2, pp. 994–1034, 2022.
- [8] F. Liu, C. Masouros, A. Li, H. Sun, and L. Hanzo, "MU-MIMO communications with MIMO radar: From co-existence to joint transmission," *IEEE Transactions on Wireless Communications*, vol. 17, no. 4, pp. 2755–2770, 2018.
- [9] S. M. Kay, *Fundamentals of statistical signal processing: Estimation theory*. Prentice-Hall, Inc., 1993.
- [10] J. Li, L. Xu, P. Stoica, K. W. Forsythe, and D. W. Bliss, "Range compression and waveform optimization for MIMO radar: A Cramér-Rao bound based study," *IEEE Transactions on Signal Processing*, vol. 56, no. 1, pp. 218–232, 2007.
- [11] Z. Ni, J. A. Zhang, K. Yang, X. Huang, and T. A. Tsiftsis, "Waveform optimization with multiple performance metrics for broadband joint communication and radar sensing," *arXiv preprint arXiv:2011.10943*, 2020.
- [12] S. D. Liyanaarachchi, T. Riihonen, C. B. Barneto, and M. Valkama, "Optimized waveforms for 5G–6G communication with sensing: Theory, simulations and experiments," *IEEE Transactions on Wireless Communications*, vol. 20, no. 12, pp. 8301–8315, 2021.
- [13] Z.-Q. Luo, W.-K. Ma, A. M.-C. So, Y. Ye, and S. Zhang, "Semidefinite relaxation of quadratic optimization problems," *IEEE Signal Processing Magazine*, vol. 27, no. 3, pp. 20–34, 2010.
- [14] C. Liu and N. Boumal, "Simple algorithms for optimization on Riemannian manifolds with constraints," *Applied Mathematics & Optimization*, vol. 82, no. 3, pp. 949–981, 2020.
- [15] M. D. Larsen, A. L. Swindlehurst, and T. Svantesson, "Performance bounds for MIMO-OFDM channel estimation," *IEEE Transactions on Signal Processing*, vol. 57, no. 5, pp. 1901–1916, 2009.
- [16] F. Wen, H. Wymeersch, B. Peng, W. P. Tay, H. C. So, and D. Yang, "A survey on 5G massive MIMO localization," *Digital Signal Processing*, vol. 94, pp. 21–28, 2019.
- [17] H.-G. Beyer and B. Sendhoff, "Robust optimization—a comprehensive survey," *Computer methods in applied mechanics and engineering*, vol. 196, no. 33–34, pp. 3190–3218, 2007.
- [18] J. R. Shewchuk, "An introduction to the conjugate gradient method without the agonizing pain," 1994.
- [19] M. ApS, *The MOSEK optimization toolbox for MATLAB manual. Version 9.0.*, 2019. [Online]. Available: <http://docs.mosek.com/9.0/toolbox/index.html>
- [20] J. Townsend, N. Koep, and S. Weichwald, "Pymanopt: A python toolbox for optimization on manifolds using automatic differentiation," *Journal of Machine Learning Research*, vol. 17, no. 137, p. 1–5, 2016. [Online]. Available: <http://jmlr.org/papers/v17/16-177.html>